Theory and simulations of quantum glass forming liquids

Thomas E. Markland, Joseph A. Morrone, Kunimasa Miyazaki, B. J. Berne, David R. Reichman et al.

Additional information on J. Chem. Phys.

Journal Homepage: http://jcp.aip.org/

Journal Information: http://jcp.aip.org/about/about_the_journal

Top downloads: http://jcp.aip.org/features/most_downloaded

Information for Authors: http://jcp.aip.org/authors

Theory and simulations of quantum glass forming liquids

Thomas E. Markland,[1] Joseph A. Morrone,[2] Kunimasa Miyazaki,[3] B. J. Berne,[2,a)]
David R. Reichman,[2,a)] and Eran Rabani[4,a)]
[1]*Department of Chemistry, Stanford University, Stanford, California 94305-5080, USA*
[2]*Department of Chemistry, Columbia University, 3000 Broadway, New York, 10027, USA*
[3]*Institute of Physics, University of Tsukuba, Tennodai 1-1-1, Tsukuba 305-8571, Japan*
[4]*School of Chemistry, The Sackler Faculty of Exact Sciences, Tel Aviv University, Tel Aviv 69978, Israel*

A comprehensive microscopic dynamical theory is presented for the description of quantum fluids as they transform into glasses. The theory is based on a quantum extension of mode-coupling theory. Novel effects are predicted, such as reentrant behavior of dynamical relaxation times. These predictions are supported by path integral ring polymer molecular dynamics simulations. The simulations provide detailed insight into the factors that govern slow dynamics in glassy quantum fluids. Connection to other recent work on both quantum glasses as well as quantum optimization problems is presented. © *2012 American Institute of Physics*. [http://dx.doi.org/10.1063/1.3684881]

I. INTRODUCTION

Understanding the fundamental causes of the dramatic slowdown of dynamics when a liquid transforms into a glass is still a subject of great debate.[1–4] Essentially all discussion of the glass transition has focused on the strictly classical regime of liquid state behavior, namely where the de Broglie wavelength is significantly smaller than the particle size. Given that nearly all known glass forming liquids fall well within this regime,[5] it is clear that the classical approximation is generally justified. However, there are several interesting and important examples where quantum fluctuations and glassiness coexist.[6,7] In such cases, which range from the behavior of superfluid helium under high pressure to the phase diagram of quantum random optimization problems, the interplay between quantum mechanics and the otherwise classical fluctuations that lead to vitrification can be expected to produce qualitatively novel physical behavior.[8]

The theoretical investigation of quantum glasses has increased in recent years. Studies ranging from the investigation of quantum effects in so-called stripe glasses,[9] quantum spin-glasses,[10–16] and lattice models that mimic the properties of superfluid and supersolid helium[17] have been presented. In this work, we instead focus on "realistic" off-lattice quantum fluids. The microscopic detail of our study necessitates the use of approximations, such as mode-coupling theory (MCT)[18] and ring-polymer molecular dynamics (RPMD),[19] that are less well-justified than the methods employed in the studies of the model systems mentioned above. On the other hand, the approaches used here have led to a host of non-trivial predictions both for classical glass-forming liquids[18] as well as a variety of quantum liquid-state phenomena.[20] We thus expect that the predictions made in this work to be at least of qualitative accuracy.

The work presented here builds on our earlier report of several novel effects that arise when glassy dynamics occurs in the quantum regime.[8] In particular, both RPMD and the quantum version of mode-coupling theory (QMCT) indicate that the dynamical phase diagram of glassy quantum fluids is reentrant. As a consequence, hard-sphere quantum liquids may be forced deeper into the glass "phase" at fixed volume fraction as quantum fluctuations increase. This counterintuitive finding has implications not only for liquid-state systems such as superfluid helium under pressure, but for a broad class of quantum optimization problems as well.

In comparison to our earlier paper,[8] the work presented here provides complete details for both the QMCT and the quantum integral equations needed for generating the required structural input. In addition, we give a far more extensive interpretation of the results, largely afforded by our RPMD simulations. Finally, we discuss in greater detail the connection of our results to related theoretical work.

The paper is organized as follows: In Sec. II, we provide the details of the QMCT, including a description of the equations for the density correlator and the mode coupling approximations. In addition, we discuss the high and low temperature limit of the QMCT and derive equations for the nonergodic parameter used to determine the liquid-glass line. In Sec. III, we describe the quantum integral equation theory used to obtain the static input required by QMCT. Section IV is devoted to the RPMD method. Results and discussions are presented in Sec. VI. Finally, in Sec. VII, we conclude.

II. A SELF-CONSISTENT QUANTUM MODE-COUPLING THEORY

The general quantity of interest is the Kubo transform[21] of the time correlation of the collective density operator, $\hat{\rho}_{\mathbf{q}} = \sum_{\alpha=1}^{N} e^{i\mathbf{q}\cdot\hat{\mathbf{r}}_\alpha}$, given by

$$\phi_q(t) = \frac{1}{N\hbar\beta} \int_0^{\hbar\beta} d\lambda \langle \hat{\rho}_q^\dagger(t+i\lambda)\hat{\rho}_q(0)\rangle$$

$$\equiv \frac{1}{N}(\hat{\rho}_q(t)|\hat{\rho}_q(0)), \tag{1}$$

a)Authors to whom correspondence should be addressed. Electronic mail: bb8@columbia.edu, drr2103@columbia.edu, and rabani@tau.ac.il.

with a time evolution described by the *exact* quantum generalized Langevin equation (QGLE),[20]

$$\ddot{\phi}_q(t) + \Omega_q^2 \phi_q(t) + \int_0^t d\tau\, M_q(\tau)\dot{\phi}_q(t-\tau) = 0. \quad (2)$$

In the above, we have used the notion that $\hat{\mathbf{r}}_\alpha$ stands for the position vector operator of particle α with a conjugate momentum $\hat{\mathbf{p}}_\alpha$ and mass m, N is the total number of particles, $\beta = 1/k_B T$ is the inverse temperature and $\langle \ldots \rangle$ in Eq. (1) denotes a quantum mechanical ensemble average. The frequency and memory terms are given by

$$\Omega_q^2 = \frac{q^2}{m\beta\phi_q(0)}, \quad (3)$$

$$M_q(t) = \frac{(Q_1 \mathcal{L}^2 \hat{\rho}_q | e^{i\bar{\mathcal{L}}t} | Q_1 \mathcal{L}^2 \hat{\rho}_q)}{\Omega_q^2 \phi_q(0)}, \quad (4)$$

respectively, with $\mathcal{L} = 1/\hbar[\hat{H}, \cdots]$ being the Liouvillian and $\bar{\mathcal{L}} = Q_2 Q_1 \mathcal{L} Q_1 Q_2$. To derive the above equations we have defined two projection operators (first and second order, respectively)[22,23]

$$P_1 = |\hat{\rho}_q)\phi_q^{-1}(0)(\hat{\rho}_q|, \quad (5)$$

$$P_2 = |Q_1 \mathcal{L}\hat{\rho}_q)(Q_1 \mathcal{L}\hat{\rho}_q|Q_1 \mathcal{L}\hat{\rho}_q)^{-1}(Q_1 \mathcal{L}\hat{\rho}_q|, \quad (6)$$

with $Q_1 = 1 - P_1$ and $Q_2 = 1 - P_2$. $\phi_q(0)$ is the zero time value of $\phi_q(t)$ and can be approximated by[22] $2S_q/\beta\hbar\Delta n(\Omega_q)\Omega_q$, where S_q is the static structure factor, $\Delta n(\omega) = n(\omega) - n(-\omega)$, and $n(\omega) = 1/e^{\beta\hbar\omega} - 1$ is the Bose distribution function at temperature T.

A. Quantum mode-coupling approach

We employ a quantum mode-coupling approach recently described by us for quantum liquids[24] to obtain the memory kernel described by Eq. (4). This approach is based on our early work to describe density fluctuations and transport in quantum liquids such as liquid *para*-hydrogen, *ortho*-deuterium, and normal liquid helium.[25–33] The basic idea behind this approach is that the random force projected correlation function, which determines the memory kernel for the intermediate scattering function, decays at intermediate and long times predominantly into modes which are associated with quasi-conserved dynamical variables. It is reasonable to assume that the decay of the memory kernel at long times will be governed by those modes that have the longest relaxation time. Thus, the first approximation made by the QMCT is to replace the projected time evolution operator, $e^{i\bar{\mathcal{L}}t}$, by its projection onto the subspace spanned by these slow modes.[20] The second approximation involves the factorization of four-point density correlations into a product of two-point density correlation.[20]

Following the derivation outlined by Götze and Lücke (GL) for zero temperature,[22,34] the memory kernel at finite temperature (in frequency space), $\tilde{M}_q(\omega)$

$= \int_{-\infty}^{\infty} dt e^{-i\omega t} M(q,t))$, can be approximated by

$$\tilde{M}_q(\omega) \approx \frac{\hbar m\beta^2}{4\pi\omega q^2 n} \int \frac{d^3k}{(2\pi)^3} V_{q,k,q-k}^2 \int_{-\infty}^{\infty} d\omega'\omega'$$
$$\times (\omega - \omega')T(\omega', \omega - \omega')\tilde{\phi}_{q-k}(\omega')\tilde{\phi}_k(\omega - \omega'), \quad (7)$$

where n is the number density, $\tilde{\phi}_q(\omega) = \int_{-\infty}^{\infty} dt e^{i\omega t} \phi_q(t)$ is the Fourier transform of the Kubo transform of the intermediate scattering function and

$$T(\omega_1, \omega_2) = n(-\omega_1)n(-\omega_2) - n(\omega_1)n(\omega_2). \quad (8)$$

The vertex, $V_{q,k,q-k}$, is formally given by

$$N_{q-k,k}V_{q,k,q-k} = (Q\mathcal{L}^2\hat{\rho}_q|\hat{\rho}_k\hat{\rho}_{q-k})$$
$$= (\mathcal{L}^2\hat{\rho}_q|\hat{\rho}_k\hat{\rho}_{q-k}) - \Omega_q^2(\hat{\rho}_q|\hat{\rho}_k\hat{\rho}_{q-k}), \quad (9)$$

with the normalization approximated by

$$N_{q-k,k} = (\hat{\rho}_q\hat{\rho}_{q-k}|\hat{\rho}_{q-k}\hat{\rho}_k)(0)$$
$$\approx \hbar\beta \int_{-\infty}^{\infty} \frac{d\omega}{\pi} \int_{-\infty}^{\infty} \frac{d\omega'}{\pi} \frac{1}{4\omega}T(\omega', \omega - \omega')$$
$$\times \omega'(\omega - \omega')\tilde{\phi}_{q-k}(\omega')\tilde{\phi}_k(\omega - \omega'), \quad (10)$$

consistent with the spirit of QMCT where four-point density correlations are factorized into a product of two-point density correlations.[20]

B. The vertex

The vertex in Eq. (9) is difficult to compute since it involves three-point Kubo density correlations. A common approach taken by classical mode-coupling theory (CMCT) is based on a convolution approximation.[35] For the Kubo transform quantum case, a convolution-like approach is not unique. The approach we adopt here is based on an extension of the work of GL to finite temperatures.[22,34] In this work, a dynamical approximation is made to remove the dependence on Kubo transformed structure factor in the vertex. The assumption behind this approximation is that the major contribution to the vertex and its normalization comes from a characteristic frequency of the system. Thus, we approximate $\tilde{\phi}_q(\omega)$ within the vertex by

$$\tilde{\phi}_q(\omega) = \frac{2\pi S_q}{\beta\hbar\Delta n(\Omega_q)\omega}(\delta(\omega - \Omega_q) - \delta(\omega + \Omega_q)). \quad (11)$$

which satisfies the known sum rule $\int_{-\infty}^{\infty} d\omega\tilde{\phi}_q(\omega) = \phi_q(0)$. Inserting this approximation for $\tilde{\phi}_q(\omega)$ into the expression for $N_{q-k,k}$ given by Eq. (10) yields

$$N_{q-k,k} \approx \frac{2S_{q-k}S_k}{\hbar\beta\Delta n(\Omega_{q-k})\Delta n(\Omega_k)}K(\Omega_{q-k}, \Omega_k), \quad (12)$$

where

$$K(\Omega_{q-k}, \Omega_k) = \frac{T(\Omega_{q-k}, \Omega_k)}{\Omega_{q-k} + \Omega_k} + \frac{T(-\Omega_{q-k}, \Omega_k)}{\Omega_{q-k} - \Omega_k}. \quad (13)$$

For $V_{q,k,q-k}$ we use the exact relations[24]

$$(L^2\hat{\rho}_q|\hat{\rho}_k\hat{\rho}_{q-k}) = \frac{1}{m\beta}(q \cdot k S_{q-k} + q \cdot (q-k)S_k), \quad (14)$$

and the convolution approximation

$$\langle \hat{\rho}_q^\dagger, \hat{\rho}_k \hat{\rho}_{q-k}\rangle \approx S_q S_k S_{q-k} \quad (15)$$

to obtain the approximation to the vertex

$$V_{q,k,q-k} = \frac{\Delta n(\Omega_{q-k})\Delta n(\Omega_k)C_{q,k,q-k}}{S_{q-k}S_k K(\Omega_{q-k},\Omega_k)}\left[\frac{(\Omega_k+\Omega_{q-k})^2-\Omega_q^2}{(\Omega_k+\Omega_{q-k})}\right], \quad (16)$$

where

$$C_{q,k,q-k} = \frac{\Omega_q S_q S_k S_{q-k} - \frac{\hbar\Delta n(\Omega_q)}{2m}[q\cdot k S_{q-k}+q\cdot(q-k)S_k]}{\Omega_q\Delta n(\Omega_k+\Omega_{q-k})-(\Omega_k+\Omega_{q-k})\Delta n(\Omega_q)}. \quad (17)$$

The above expressions close the equation of motion (Eq. (2)) and require only the static structure factor to produce a full approximation to the time dependence of the quantum density-density time autocorrelation function.

C. High and low temperature limits

It may be shown that the above equations reduce to the venerable classical mode-coupling equations in the high temperature limit and to the GL theory as $T \to 0$. The latter theory produces a representation of the dispersion of superfluid helium that is at least as accurate as the Feynman-Cohen (FC) theory[36] at low values of q and exhibits Pitaevskii-bending of the spectrum at high q, unlike the FC theory. In particular at high T,

$$\lim_{\beta\to 0} M_q(t) \approx \frac{k_B T n}{16\pi^3 m q^2}\int d^3k\,(q\cdot k c_k$$
$$+ q\cdot(q-k)c_{q-k})^2\phi_{q-k}(t)\phi_k(t), \quad (18)$$

where $c_q = 1/n(1 - 1/S_q)$ is the direct correlation function. In addition, $\phi_q(t)$ reduces to the classical intermediate scattering function, $F(q, t)$ as $\beta \to 0$. This is recognized as the CMCT memory function.[18]

At $T \to 0$ the equation for the memory function reduces to

$$\lim_{T\to 0} \tilde{M}_q(\omega) \approx \frac{\hbar m\beta^2}{2n\omega q^2}\int \frac{d^3k}{(2\pi)^3}V_{q,k,q-k}^2$$
$$\times \int_0^\omega \frac{d\omega'}{\pi}\omega'(\omega-\omega')\tilde{\phi}_{q-k}(\omega')\tilde{\phi}_k(\omega-\omega'), \quad (19)$$

with

$$\lim_{T\to 0} V_{q,k,q-k} = \frac{\hbar n}{2m}(\omega_k + \omega_{q-k} + \omega_q)$$
$$\times(q\cdot k c_k + q\cdot(q-k)c_{q-k}), \quad (20)$$

which are the $T \to 0$ equations for quantum density fluctuations in superfluid helium first derived by GL.[22,34] In the above, $\omega_q = \hbar q^2/2mS_q$. We note in passing that the term β^2 appearing in Eq. (19) (and not in the derivation of GL) arises

from our definition of the Kubo transform (Eq. (1)), which includes a $1/\hbar\beta$, while that of GL does not. Care must be taken applying the Kubo transform as $T \to 0$.

In the $T \to 0$ case, the entire structure of the memory function differs greatly from that of its high temperature counterpart and the convolution structure is lost. Equations (19) and (20) do not imply a memory function that is a product of correlators at identical times. This is a consequence of the quantum fluctuation-dissipation theorem that must be satisfied. At $T \to 0$ the function $T(\omega_q, \omega_k)$ becomes proportional to the difference of a product of step-functions in frequency, dramatically altering the structure of the theory. This distinction between the low and high temperature limits has important consequences, as discussed below.

D. Nonergodic parameter

The nonergodic parameter,

$$f_q = \frac{\phi_q(t \to \infty)}{\phi_q(0)} = \frac{\hbar\Delta n(\Omega_q)\Omega_q}{2k_B T S_q}\phi_q(t \to \infty), \quad (21)$$

is often used to describe the ergodic to nonergodic transition as the liquid is cooled down to the mode-coupling critical temperature T_c. Above T_c one finds a single solution where $f_q = 0$ for all values of q, while at T_c the nonergodic parameter acquires a finite value $f_q > 0$.[37] It is simple to show that f_q must satisfy the equation[38]

$$\frac{f_q}{1-f_q} = \frac{1}{\Omega_q^2}M_q(t \to \infty). \quad (22)$$

The above equation for the nonergodic parameter reflects the structure of the QGLE (Eq. (2)), and thus, is valid both in the classical and quantum limits. In the former, the long time limit of the memory kernel is given by $M_q(t \to \infty) \approx (k_B T n/16\pi^3 m q^2)\int d^3k\,\bar{V}_{q,k,q-k}^2 f_{q-k}f_k$ with $\bar{V}_{q,k,q-k}^2 = S_{q-k}S_k(q\cdot k c_k + q\cdot(q-k)c_{q-k})^2$. The quantum case is a bit more complicated since the structure of the memory kernel is quite different and involves a convolution of products of $\tilde{\phi}_q(\omega)$. The derivation for $M_q(t \to \infty)$ is thus, based on the following expansion:

$$\frac{1}{\omega}T(\omega',\omega-\omega')\omega'(\omega-\omega')$$

$$= \frac{1}{\beta\hbar}+\frac{\beta\hbar}{12}\omega'(\omega-\omega')-\frac{(\beta\hbar)^3}{720}(\omega'^2-\omega'(\omega-\omega')+(\omega-\omega')^2)$$

$$\times \frac{(\beta\hbar)^5}{30240}((\omega-\omega')^4 - \omega'(\omega-\omega')^3 + \omega'^2(\omega-\omega')^2$$
$$-\omega'^3(\omega-\omega') + \omega'^4) + O(\beta^7). \quad (23)$$

Inserting this into the memory kernel (Eq. (7)) and keeping the first two terms only, we obtain

$$\tilde{M}_q(\omega) \approx \frac{\hbar m\beta^2}{4\pi q^2 n}\int \frac{d^3k}{(2\pi)^3}V_{q,k,q-k}^2\int_{-\infty}^\infty d\omega'$$

$$\times\left(\frac{1}{\beta\hbar}+\frac{\beta\hbar}{12}\omega'(\omega-\omega')+\cdots\right)\tilde{\phi}_{q-k}(\omega')\tilde{\phi}_k(\omega-\omega'). \quad (24)$$

In the time domain, this translates to

$$M_q(t) \approx \frac{\hbar m \beta^2}{2q^2 n} \int \frac{d^3 k}{(2\pi)^3} V_{q,k,q-k}^2$$
$$\times \left(\frac{1}{\beta \hbar} \phi_{q-k}(t) \phi_k(t) + \frac{\beta \hbar}{12} \dot{\phi}_{q-k}(t) \dot{\phi}_k(t) + \cdots \right),$$
$$(25)$$

where the dot denotes a time derivative, i.e., $\dot{\phi}_k(t) = d\phi_k(t)/dt$. The other terms in the expansion of Eq. (23) that have been omitted give rise to terms of the form

$$\sum_j a_j(\beta) \phi_{q-k}^{(j)}(t) \phi_k^{(n-j)}(t),$$
$$(26)$$

where $a_j(\beta)$ are related to the expansion coefficients of $(1/\omega)T(\omega', \omega - \omega')\omega'(\omega - \omega')$ and $\phi_k^{(j)}(t) = d^j \phi_k(t)/dt^j$ is the j's time derivative of $\phi_k(t)$.

The long time limit of Eq. (25) is now given by

$$M_q(t \to \infty) \approx \frac{m\beta}{2q^2 n} \int \frac{d^3 k}{(2\pi)^3} V_{q,k,q-k}^2$$
$$\times \phi_{q-k}(t \to \infty) \phi_k(t \to \infty),$$
$$(27)$$

where all the time derivatives vanish as $t \to \infty$ even when $\phi_k(t \to \infty)$ decays to a constant. Finally, we can rewrite the above in terms of the nonergodic parameter

$$M_q(t \to \infty) \approx \frac{m\beta}{2q^2 n} \int \frac{d^3 k}{(2\pi)^3}$$
$$\times V_{q,k,q-k}^2 \phi_{q-k}(0) \phi_k(0) f_{q-k} f_k.$$
$$(28)$$

The above expression is strictly valid at $T \to 0$ but not at $T = 0$, since the expansion given by Eq. (23) is not valid at $T = 0$. The final result is similar to the classical equation, however, the vertex is given by the full quantum mechanical expression of Eq. (16).

III. QUANTUM INTEGRAL EQUATION THEORY

The QMCT requires as input the static structure factor, S_q and its Kubo transform $\phi_q(0)$. Here, instead of using path integral Monte Carlo to generate this input,[39] we refer to a quantum integral equation approach, that is based on the early work of Chandler and Richardson.[40, 41] We begin with the Ornstein-Zernike relation applicable to quantum liquids. The quantum system composed of N particles can be mapped on a classical system consisting of N ring polymers, each polymer being composed of P beads. Then, we can write the matrix reference interaction site model (RISM)[40,41] equation for the classical isomorphic system by

$$h(|\mathbf{r} - \mathbf{r}'|) = w * c * w(|\mathbf{r} - \mathbf{r}'|) + nw * c * h(|\mathbf{r} - \mathbf{r}'|),$$
$$(29)$$

where * denotes a convolution integral and as before, n is the number density. In the above equation, $h(r)$, $w(r)$, and $c(r)$ are the total correlation function, the self correlation function, and the

direct correlation function, respectively, defined by

$$h(r) = \frac{1}{\hbar\beta} \int_0^{\hbar\beta} d\lambda h(r, \lambda), \quad w(r) = \frac{1}{\hbar\beta} \int_0^{\hbar\beta} d\lambda w(r, \lambda),$$

$$c(r) = \frac{1}{\hbar\beta} \int_0^{\hbar\beta} d\lambda c(r, \lambda),$$
$$(30)$$

and $h(r, \lambda)$, $w(r, \lambda)$, and $c(r, \lambda)$ are the imaginary time total, self, and direct correlation functions, respectively. In the classical limit, Eq. (29) reduces to the classical Ornstein-Zernike equation with $w(r) = 1$. In what follows, we will use the notation $\tilde{w}_q(\lambda)$ for the Fourier transform of $w(r, \lambda)$, and similarly for $\tilde{c}_q(\lambda)$ and $\tilde{h}_q(\lambda)$:

$$\tilde{h}_q = \frac{1}{\hbar\beta} \int_0^{\hbar\beta} d\lambda \tilde{h}_q(\lambda), \quad \tilde{w}_q = \frac{1}{\hbar\beta} \int_0^{\hbar\beta} d\lambda \tilde{w}_q(\lambda),$$

$$\tilde{c}_q = \frac{1}{\hbar\beta} \int_0^{\hbar\beta} d\lambda \tilde{c}_q(\lambda).$$
$$(31)$$

To proceed, we refer to the mean-pair interaction approximations along with the quadratic reference action[40] and rewrite

$$\tilde{w}_q(\lambda) = \exp\{-q^2 R^2(\lambda)\},$$
$$(32)$$

where

$$R^2(\lambda) = \sum_j \frac{1 - \cos(\Omega_j \lambda)}{\beta m \Omega_j^2 + \alpha_j},$$
$$(33)$$

m is the particle mass, $\Omega_j = 2\pi j/\hbar\beta$ is the Matsubara frequency and α_j is given by

$$\alpha_j = \frac{1}{6\pi^2 \hbar\beta} \int_0^\infty dq \int_0^{\hbar\beta} d\lambda q^4 \tilde{v}_q (1 - \cos(\Omega_j \lambda) \tilde{w}_q(\lambda).$$
$$(34)$$

In the above the solvent induced self-interaction is given by

$$\tilde{v}_q = -\tilde{c}_q^2 (n\tilde{w}_q + n^2 \tilde{h}_q).$$
$$(35)$$

In order to close the quantum Ornstein-Zernike equations, which in q-space can be written as

$$\tilde{h}_q = \tilde{w}_q \tilde{c}_q \tilde{w}_q + n\tilde{w}_q \tilde{c}_q \tilde{h}_q,$$
$$(36)$$

we use the Percus-Yevick (PY) closure of the form (in r-space)

$$c(r) = (h(r) + c(r) + 1)(\exp(-\beta v(r)) - 1),$$
$$(37)$$

where $v(r)$ is the pair interaction between two particles. The static structure factor and its Kubo transform are then given by

$$S_q = 1 + n\tilde{h}_q, \quad \phi_q(0) = \tilde{w}_q + n\tilde{h}_q.$$
$$(38)$$

In all the applications reported below we have used the approximate relation for $\phi_q(0) \approx 2S_q/\beta\hbar\Delta n(\Omega_q)\Omega_q$.

IV. RING POLYMER MOLECULAR DYNAMICS

The RPMD approach to quantum dynamics provides an approximation to quantum mechanical Kubo transformed correlation functions by using a classical evolution of the imaginary time paths.[19] Consider a multidimensional system of N

distinguishable particles with a Hamiltonian of the form,

$$H = \sum_{\alpha=1}^{N} \frac{\mathbf{p}_{\alpha}^2}{2m_{\alpha}} + V(\mathbf{r}_1, \ldots, \mathbf{r}_N), \qquad (39)$$

where $\mathbf{r}_{\alpha}$ and $\mathbf{p}_{\alpha}$ are the positions and momenta of the particles and $V(\mathbf{r}_1, \ldots, \mathbf{r}_N)$ is the potential energy of the system. The RPMD approximation to the canonical correlation function, $\tilde{c}_{AB}(t)$, for position dependent operators $A(\mathbf{r})$ and $B(\mathbf{r})$ is

$$\tilde{c}_{AB}(t) \simeq \frac{1}{(2\pi\hbar)^{3NP} Z_P} \int d^{3NP}\mathbf{p} \int d^{3NP}\mathbf{r}$$
$$\times e^{-\beta_P H_P(\mathbf{p},\mathbf{r})} A_P(\mathbf{r}) B_P(\mathbf{r}_t), \qquad (40)$$

where

$$Z_P = \frac{1}{(2\pi\hbar)^{3NP}} \int d^{3NP}\mathbf{p} \int d^{3NP}\mathbf{r}\, e^{-\beta_P H_P(\mathbf{p},\mathbf{r})}, \qquad (41)$$

and $\beta_P = \beta/P$. $H_P(\mathbf{p}, \mathbf{r})$ is the classical Hamiltonian of the N particle P bead ring polymers with the external potential of $V(\mathbf{r}_1, \ldots, \mathbf{r}_N)$ acting on each bead,

$$H_P(\mathbf{p}, \mathbf{r}) = \sum_{\alpha=1}^{N} \sum_{k=1}^{P} \left(\frac{(\mathbf{p}_{\alpha}^{(k)})^2}{2m_i} + \frac{1}{2} m_{\alpha} \omega_P^2 (\mathbf{r}_{\alpha}^{(k)} - \mathbf{r}_{\alpha}^{(k+1)})^2 \right)$$
$$+ \sum_{k=1}^{P} V(\mathbf{r}_1^{(k)}, \ldots, \mathbf{r}_N^{(k)}), \qquad (42)$$

where $\omega_P = 1/\beta\hbar$ and the cyclic boundary condition $\mathbf{r}_{\alpha}^{(P+1)} \equiv \mathbf{r}_{\alpha}^{(1)}$ applies. The time-evolved coordinates $\mathbf{r}_t \equiv \mathbf{r}_t(\mathbf{p}, \mathbf{r})$ in Eq. (40) are obtained from the classical dynamics generated from this Hamiltonian and the operators $A_P(\mathbf{r})$ and $B_P(\mathbf{r}_t)$ are evaluated by averaging over the beads of the ring polymer at times 0 and t, respectively,

$$A_P(\mathbf{r}) = \frac{1}{P} \sum_{k=1}^{P} A(\mathbf{r}_1^{(k)}, \ldots, \mathbf{r}_N^{(k)}), \qquad (43)$$

$$B_P(\mathbf{r}) = \frac{1}{P} \sum_{k=1}^{P} B(\mathbf{r}_1^{(k)}, \ldots, \mathbf{r}_N^{(k)}). \qquad (44)$$

The RPMD method has previously been used to study a diverse selection of multidimensional systems including proton transfer between organic molecules,[42] diffusion in and inelastic neutron scattering from liquid para-hydrogen,[43,44] diffusion of light atoms in liquid water,[45] and gas phase reactions such as that between methane and hydrogen.[46] In all cases RPMD has been able to capture the dominant quantum mechanical effects in the dynamics and provide good agreement with the available experimental or exact results. RPMD has also been applied to look at deep tunneling of muonium and hydrogen atoms in ice[45] and in this regime has been shown to be related to semi-classical instanton theory.[47]

V. SIMULATIONS DETAILS

The quantum mode coupling theory requires as input the static structure factor and its Kubo transform. In the present study, we used a single component hard sphere (HS) model

TABLE I. Parameters used in our RPMD simulations on the Andersen-Kob Lennard-Jones glass forming system.

Parameter	LJ units	Atomic units
ϵ_{AA}	1	3.8×10^{-4}
ϵ_{BB}	0.5	1.9×10^{-4}
ϵ_{AB}	1.5	5.7×10^{-4}
σ_{AA}	1	6.43
σ_{BB}	0.88	5.65
σ_{AB}	0.8	5.14
Mass$_A$	1	3646
Mass$_B$	1	3646

to generate this input within the framework of the integral equation approach described above. Using the PY closure, the system remains disordered even at very high volume fraction, thus providing a simple model to explore the quantum glass transition. The integral Eqs. (31)–(34) were solved self-consistently. A simple trapezoidal integration scheme over the imaginary time axis was employed, with $P = 400$ slices (we have checked convergence of the static input with respect to P). Here, P is analogous to the number of beads in the RPMD approach. For the HS system, it can be shown that the quantum mode coupling equations scale with the ratio of the de Broglie thermal wavelength to the particle size, $\Lambda^* = \sqrt{\beta\hbar^2/m\sigma^2}$. Thus, to change the quantumness, one can either change $\hbar$, or the mass, or the temperature. For the QMCT results shown below, we have varied the temperature to reflect a change in Λ^*. We note that the temperature has no effect on the static structure factor in the classical case.

We performed RPMD simulations on the Kob-Andersen glass forming system,[48,49] a binary LJ fluid, because the HS system investigated above by means of QMCT crystallizes on the time scale of the RPMD simulations. Each simulation consisted of 1000 particles, 800 of type A and 200 of type B in a cubic box of length $9.4\sigma_{AA}$. The LJ parameters are given in Table I. The equations of motion were integrated using a time step of 0.005 in Lennard-Jones (LJ) units using the normal mode integration scheme of Ref. 50. To achieve convergence of a path integral simulation a well established criterion is that,[51]

$$P > \frac{\hbar\omega_{max}}{k_B T^*} \qquad (45)$$

where ω_{max} is the highest frequency in the system. In our simulations the number of beads, P, used was given by the formula,

$$P = \frac{11.2\hbar}{T^*}. \qquad (46)$$

This choice gives good convergence for all the regimes studied which was checked by monitoring the convergence of the potential and quantum kinetic energy of the system with respect to the number of beads for each state point simulated. Initial configurations were generated by annealing from a temperature $T^* = 5.0$ to the target temperature over a period of 2×10^6 time steps. From these initial configurations we ran a further 2×10^5 steps of equilibration using a targeted Langevin equation normal mode thermostatting scheme.[50]
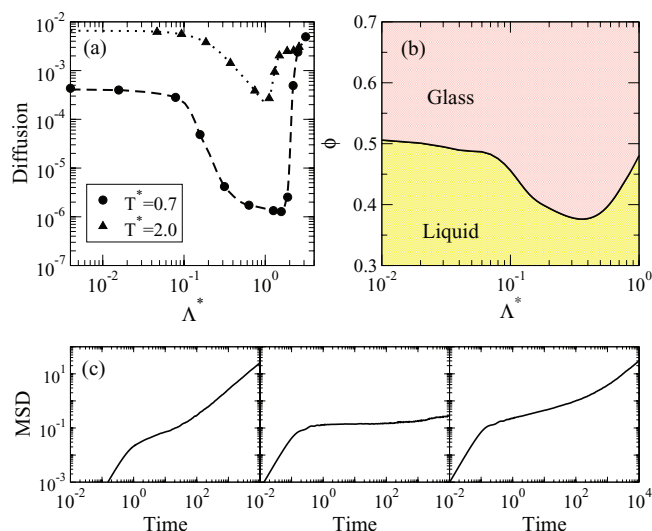
FIG. 1. Panel (a): The diffusion constant of particles of type A as a function of the quantumness, Λ^*, obtained from the RPMD simulations for a quantum Kob-Anderson LJ binary mixture for two temperatures. Panel (b): Dynamic phase diagram (volume fraction versus quantumness) calculated from the QMCT for a hard-sphere fluid. Panel (c): The mean square displacement of A particles as obtained from the RPMD simulations for the classical case (left frame, $\Lambda^* = 0$), the trapped regime (middle frame, $\Lambda^* = 1.125$), and the regime governed by strong quantum fluctuations (right frame, $\Lambda^* = 1.1325$).

This was followed by microcanonical dynamics for 2×10^6 steps during which the results were collected. In contrast to the QMCT simulations for the RPMD simulations the quantum effect was varied by varying $\hbar$. This was chosen since mass and temperature also alter the classical result whereas $\hbar$ purely changes the magnitude of the quantum fluctuations in the system. Five simulations were run for each temperature and value of $\hbar$ and the results averaged.

VI. RESULTS

Figure 1 shows the results obtained from our QMCT treatment of hard spheres and RPMD simulations of the Kob Andersen (KA) binary Lennard-Jones (LJ) fluid as the size of quantum fluctuations in the system are varied.[8] Both of these systems have previously been shown to exhibit all of the features of glassy behavior present in more complex fluids. In panel (b), we show the liquid-glass dynamic phase diagram that is obtained from the QMCT calculation. The phase boundary is defined as the point where the solution of Eqs. (21)–(28) leads to a finite value for the nonergodic parameters, f_q. At this point, QMCT predicts that the system will never fully relax on any time scale at the given packing fraction. For the RPMD calculations, which are based on the evolution of semi-classical trajectories, we instead show the effect of quantum fluctuations on the diffusion coefficient of the particles at two different temperatures ($T^* = 2.0$ and 0.7) as the classical glass transition temperature of the system is approached ($T^* \approx 0.45$) in panel (a) of Fig. 1. Since the mean square displacement of the particles in the ring polymer trajectories show a caging regime (see the panel (c) of Fig. 1), the diffusion constant was extracted from the long time slope of the mean-square displacement where the diffusive regime

had been reached. The size of the quantum fluctuations were controlled by varying Λ^*, the ratio of the de Broglie thermal wavelength to the particle size which controls the scale of quantum behavior.

Comparing the RPMD results in panel (a) and QMCT results in panel (b) of Fig. 1, a remarkably consistent picture emerges from these two different approaches to quantum dynamics and glass forming systems. In the classical limit ($\Lambda^* \rightarrow 0$), RPMD reduces to classical mechanics and QMCT to classical MCT. As small quantum fluctuations are initially introduced, little difference is observed in either the RPMD diffusion coefficient or QMCT liquid-glass line. However, as Λ^* is increased beyond 0.1, quantum effects are at first found to promote and then inhibit glass formation. In the case of RPMD, this is characterized by a decrease of nearly three orders of magnitude in the diffusion coefficient, and for QMCT, a 20% fall in the packing fraction required for vitrification. When the thermal wavelength is increased further and becomes on the order of the particle size, the diffusion coefficient in the quantum system exceeds that observed in the classical limit. In addition, the RPMD simulations at $T^* = 0.7$ and 2.0 indicate that size of the re-entrance becomes much larger as the glass transition temperature is approached. Moreover, there is a hint of an interesting effect where, at high values of Λ^*, the diffusion coefficient at lower temperature exceeds that at the higher temperature. We will return to this point later.

Since both MCT and our new QMCT approach use the structure factor as input it is instructive to see if the dynamical reentrance is hinted at in this property. Figure 2 shows the radial distribution function (RDF), which is the spatial Fourier transform of the structure factor, that has been calculated from the RPMD simulations of the Kob Andersen Lennard-Jones (KALJ) fluid. For static equilibrium properties such as the RDF, RPMD gives numerically exact results since it reduces to the path integral molecular dynamics approach.[52] The true (observable) quantum RDF is determined by the ring polymer bead correlations and is shown in the top panel for both the classical limit ($\Lambda^* = 0$) and for a trapped regime ($\Lambda^* = 0.75$). As quantum effects are introduced, the RDF exhibits a broadening of the peaks due to the increasing uncertainty in the particle positions which acts to smear out the pair structure. Throughout the entire range of Λ^* studied the structure is observed simply to broaden systematically with Λ^* and thus, there is no indication of the observed dynamical reentrance in the RDF.

In the bottom panel, we show the centroid RDF in which the centers of the imaginary time paths, rather than the bead positions, were used to compute the RDF. In the classical limit all beads collapse to a single point and hence both ways of calculating the RDF become identical. However as quantum fluctuations are increased the beads spread further from the center of the polymer and hence the centroid structure offers a different view into the structure of the quantum liquid. Upon examining the centroid RDF in Fig. 2, one sees the opposite trend upon increasing quantum fluctuations to that observed in the bead RDF, i.e., weak quantum fluctuations lead to a more structured centroid RDF which one would associate with more glassy dynamics. As quantum fluctuations further increase this trend reverses (data not shown). Hence
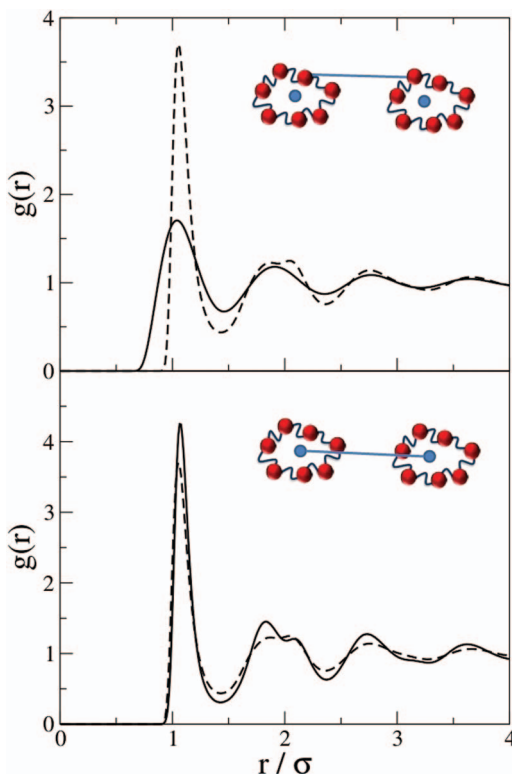
FIG. 2. The bead (upper panel) and centroid (lower panel) radial distribution functions of A particles for a classical ($\Lambda^* = 0$, dashed) and trapped quantum ($\Lambda^* = 0.75$, solid) regime. The bead distribution suggests less order in the trapped regime compared to a classical simulation while the centroid structure shows an increase in order.

FIG. 3. Root-mean-square of the radius of gyration of A particles as a function of Λ^* obtained from the RPMD simulations for a quantum Kob-Anderson LJ binary mixture for two temperatures. The radius of gyration is defined as the average distance of the replicas from the polymer center. The results are plotted for temperatures $T^* = 0.7$ (circles with dashed lines) and $T^* = 2.0$ (triangles with dotted lines).

the centroid pair distribution function, which is not an experimental observable, appears to grossly mimic the dynamical correlations observed in both the QMCT and RPMD calculations. This is not entirely surprising, because one expects that the centroid molecular dynamics (CMD) method,[53] an approach similar to RPMD, will also capture the reentrance. Since CMD is an effective classical dynamics on the many-body centroid potential and since there are situations where the many-body centroid potential can be approximated by a sum of pair-wise potentials given by $-k_B T \log g(r)$,[54,55] such static correlations in the centroid RDF must be evident if CMD is to reproduce the same phenomenology as predicted by QMCT and RPMD. This fact suggest that a strictly classical MCT calculation that uses a static structure factor constructed from the centroid correlations might be a good proxy for the full QMCT calculation. It should be noted that the full QMCT only uses the observable structure factor and thus one role played by the quantum vertex function is to effectively convert the bead correlations to centroid ones via the quantum fluctuation-dissipation theorem. The fact that the quantum vertex involves frequency convolutions while the classical version does not suggests, however, that there must be some distinction between a classical MCT calculation with centroid correlations and the full QMCT.

So what is the origin of the reentrance? For this we turn to the RPMD trajectories to provide a physically insightful picture. Since this approximation maps the dynamics of a quantum mechanic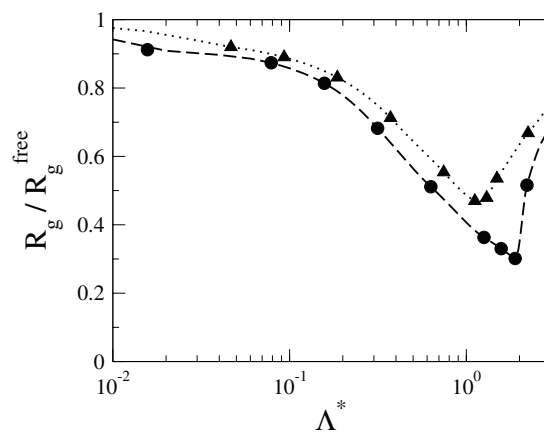al particles onto that of a system of classical ring polymers, we can initially interpret the results in the language of the diffusion of classical polymers. In doing so we are careful to note that each bead on a given polymer only interacts with the bead on another ring polymer corresponding to the same imaginary time slice, a point which we will return to later in this section. In the non-interacting limit, the free ring polymer radius of gyration is directly proportional to the thermal deBroglie wavelength of the quantum particle. Hence, increasing Λ^* allows the ring polymer representing each quantum particle to spread out. The average radius of gyration of each quantum particle in the interacting KALJ system is a static property which can be calculated exactly from RPMD simulations. In Fig. 3, we plot the average radius of gyration of each ring polymer relative to the value in the free limit. The dependence of this ratio on Λ^* mimics the dependence of the diffusion coefficient on Λ^* shown in Fig. 1. The decrease in this ratio when reentrance is observed suggests a correlation between the localization of the quantum particle and the increase in the glassiness of the system. As quantum fluctuations are increased from $\Lambda^* < 0.1$, the effective diameter of the quantum particles differ little from σ so that they can still fit into the thermally accessible space, their radius of gyration is still well approximated by R_g^{free}, and little change in the dynamics is observed. However, once Λ^* exceeds 0.1 there is not enough free space for the free ring polymers to further expand and crowding due to the surrounding solvent cage causes the radius of gyration to decrease from its free particle value.

In the upper panel of Fig. 4, we show typical configurations of a RPMD trajectory in the regime where the particle is localized in a cavity. The particle is confined by its surrounding neighbors, thus giving rise to an increase in its quantum kinetic energy. For diffusion to occur, particles must push past each other, causing further localization and incurring an even greater increase in their kinetic energies. This energy penalty to motion leads to slower dynamics. As Λ^* is further increased, a tipping point is reached when the thermal wavelength becomes comparable to the particle size, $\Lambda^* \approx 1$.
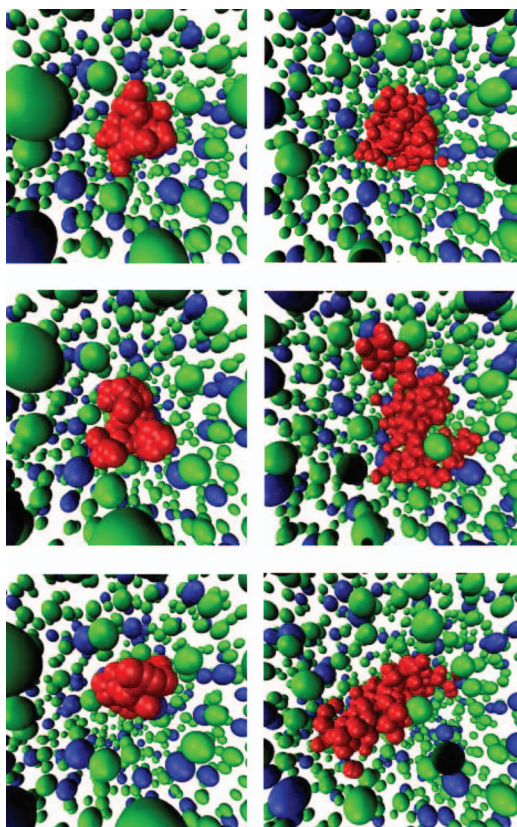
FIG. 4. A series of snapshots taken from simulations at $\Lambda^* = 1.125$ (left panels) and $\Lambda^* = 1.3125$ (right panels) with $T^* = 0.7$. For clarity the full imaginary time path (colored red) is only shown for one particle of type A with all others represented by their centroids. The centroids for the other particles of types A and B are colored green and blue, respectively. The left panels depict configurations which reside in the trapped regime where the ring polymer is essentially localized in one cavity cage whereas in the tunneling regime (right panels) it is frequently spread across two or more cavities in the liquid resulting in more facile motion.

At this point, the cost of localization becomes so large that the induced quantum kinetic energy enables the crossing of barriers between cavities, leading to a rise in the radius of gyration and facilitating diffusion. This can be seen in the representative snapshots of a RPMD trajectory shown in the lower panels of Fig. 4 in which the particle is delocalized across two cavities. Accordingly, the radius of gyration recovers with a corresponding increase in diffusion coefficient and diminishing of the caging regime. This can be likened to a "lakes to oceans" percolation transition, in which the caging regime reflects frustration of the quantum particle in the classical potential, a frustration which is reduced when the kinetic energy of confinement essentially floods the barriers and allows the particle to traverse the region between adjacent potential energy minima.

Reentrant effects in quantum systems have also been observed in the diffusion of electrons in a sea of classical random blockers[56] as well as in model systems.[9,17] In the former case, the problem can be exactly mapped onto the diffusion of a classical ring polymer. However, in our case, while the expression "ring polymer" is used to describe the isomorphism arising from the imaginary time path integral representation described in Eqs. (39)–(42), it is not simply that of a system

of true harmonic ring polymers. This is because each bead of a polymer only interacts with its corresponding bead at the same imaginary time on the polymer representing another particle and not with any other beads on that particle. One might therefore expect that in systems with strong interactions it might be advantageous for the polymers to correlate their beads so as to minimize repulsion in exchange for a loss in entropy. To investigate this, we define vectors $\mathbf{R}_\alpha^k = \mathbf{r}_\alpha^{(k)} - \mathbf{r}_\alpha^c$, which represent the position of the bead at imaginary time k on ring polymer α relative to the position of the centroid ($\mathbf{r}_\alpha^c = (1/P) \sum_{k=1}^P \mathbf{r}_\alpha^{(k)}$), and we define the angle between vectors $\mathbf{R}_\alpha^k$ and $\mathbf{R}_\beta^{(k)}$ as

$$\cos \theta_{\alpha,\beta}^{(k)} = \frac{\mathbf{R}_\alpha^{(k)} \cdot \mathbf{R}_\beta^{(k)}}{|\mathbf{R}_\alpha^{(k)}| |\mathbf{R}_\beta^{(k)}|}. \tag{47}$$

This function, $\cos \theta_{\alpha,\beta}^{(k)}$, will have a value of -1 if the kth beads on polymers α and β are aligned perfectly away from each other and $+1$ if the beads are aligned towards each other. Since any correlation between the beads on two different particles is likely to be more pronounced at short distances where interactions are stronger we plot the correlation function $C(r)$,

$$C(r) = \left\langle \frac{1}{N} \sum_{\alpha > \beta} \frac{1}{P} \sum_{k=1}^P \cos \theta_{\alpha,\beta}^{(k)} \delta(r - |\mathbf{r}_{\alpha,\beta}^c|) \right\rangle, \tag{48}$$

as a function of the distance between the centroids of two ring polymers.

The function $C(r)$ is shown in Fig. 5 for $\Lambda^* = 0.75$, which corresponds to the trapped regime, and for $\Lambda = 1.3125$, which corresponds to the strong quantum fluctuation regime. For $r \leq \sigma$ $C(r)$ is negative in both cases. At these distances the potential between particles is strongly repulsive and hence for polymers to approach this close their beads for the same imaginary time must avoid each other. However for $r \approx \sigma$, $C(r)$ corresponding to the lower value of Λ^*, the correlation becomes positive. At this distance the pair potential is attractive and hence the energy of the system is lowered if the polymer arranges its beads such that they are aligned on the same side of the respective ring-polymers. However, at the higher value of Λ^*, the entropic cost of such an ordering outweighs the energetic benefit, and hence $C(r)$ is negative. This coincides with the change between the dynamical regimes of quantum trapping and strong fluctuations because, for diffusion to occur, particles must move past each other. This regime corresponds to enhanced tunneling. In the case of low Λ^* the beads of the polymer in the first coordination shell at $r = \sigma$ are largely aligned such that pushing them together induces a larger repulsion than if no such correlation existed. This increases the barrier to diffusion in this regime.

One natural question that arises from this interpretation of our results is what occurs if the RPMD calculations are carried out at constant pressure rather than constant volume. The analogous QMCT calculations are constant volume calculations and indeed, as far as the hard-sphere control variables of volume fraction and Λ^* are concerned, this question is irrelevant. The pressure varies as the volume fraction, which can then just be rescaled to yield results identical to those presented in the panel (b) of Fig. 1. However, from the
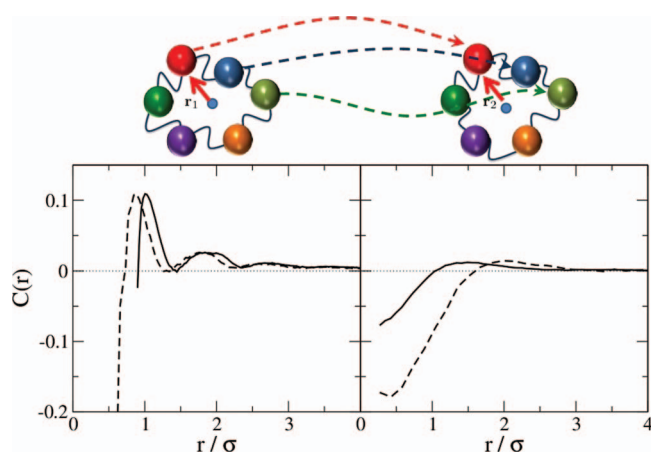
FIG. 5. The bead vector correlation (see Eq. (48)) for a trapped regime with $\Lambda^* = 0.75$ (left panel) and regime where quantum fluctuations are pronounced with $\Lambda^* = 1.3125$ (right panel). The solid lines represent the bead vector correlations between A particles and the dashed ones those between B particles. In both cases $T^* = 0.7$. In the trapped regime the ring polymer beads show a large positive correlation around $r = \sigma$ which results in a large repulsion when the particles attempt to move past each other. In the other regime the beads align such that the correlation is largely negative which facilitates particle motion.

standpoint of thermal variation, e.g., the variation of diffusion at fixed temperature while varying Λ^* (see panel (a) of Fig. 1), this question needs to be addressed. A natural expectation is that at constant pressure the reentrant effect will be mitigated or destroyed as the system can now adjust its volume as a natural response to the buildup of local pressure created by the "swelling" of the ring polymer. However, some aspects of this effect have been observed, for example, in analogous reentrant-like effects seen in Ref. 45, where quantization of a single species in a constant pressure classical bath produces a reduction of the effective diffusion constant. More generally the values of Λ^* for which the slowing of the liquid is observed are highly realizable in room temperature systems. The thermal wavelength of hydrogen at 300 K is 1.0 and hence the region of quantum slowing corresponds to diffusion in a medium with particles of radius 2 to 5. Such a slow down is evident in experimental measurements of the diffusion of hydrogen in non-glassy media such as water and palladium.[45,57]

We have carried out RPMD simulations of the binary glass-forming system at constant pressure, and indeed found at least a strong mitigation of the reentrant effect. Currently our statistics are not sufficient to make definitive statements about dynamical behavior in these systems, and thus these results will be reported in a future publication. Regardless, it is clear that constant volume (confined) systems will exhibit a strong enhancement of the effects reported here. Further it should be mentioned that a similar reentrance is seen in lattice models of quantum glasses where the concept of swelling of imaginary time paths cannot be invoked to explain reentrant relaxation.[9,17]

On a final note, a subtle feature of the RPMD results of Fig. 1 (panel (a)) should be mentioned. At very large values of Λ^* the isothermal diffusion curves appear to cross. While the effect is quite small, this crossing would imply a reentrance of a different sort, namely a "melting by cooling" mechanism.

This type of reentrance, distinct from that discussed for the bulk of this work, is similar to that discussed in Ref. 9. It should be noted, however, that the Λ^* values here are large enough that particle statistics cannot be neglected in the simulation of a realistic quantum fluid, and the inclusion of such features may obviate this effect.

VII. CONCLUDING REMARKS

In this work, we have presented a self-contained discussion of predictions for quantum glasses made by QMCT and RPMD. The predictions of these two distinct, albeit highly approximate, theories appear to be in harmony with each other. Both predict a strong reentrance in the relaxation of quantum supercooled liquids, namely that weak quantum fluctuations actually serve to push the system closer towards the glass transition. This seemingly paradoxical effect has also been noted in lattice models of quantum glasses and in models of quantum optimization. Indeed, one interesting aspect of our work is that it suggests that typical quantum annealing protocols should generically have regions of parameter space where they are in fact less efficient than their classical counterparts.

Future work will be directed towards the inclusion of bosonic statistics into the formulation of QMCT so that an investigation of the putative superglass may be carried out in a microscopic manner. In addition, it would be interesting to investigate more complex liquids such as confined supercooled water to see if quantum effects which may manifest at high temperatures lead to novel dynamical relaxation patterns. These topics will be reserved for the future.

ACKNOWLEDGMENTS

[1]P. G. Debenedetti and F. H. Stillinger, Nature (London) **410**, 259 (2001).
[2]L. Berthier, G. Biroli, J. Bouchaud, L. Cipelletti, D. El Masri, D. L'Hote, F. Ladieu, and M. Pierno, Science **310**, 1797 (2005).
[3]G. Biroli, J. P. Bouchaud, A. Cavagna, T. S. Grigera, and P. Verrocchio, Nat. Phys. **4**, 771 (2008).
[4]L. O. Hedges, R. L. Jack, J. P. Garrahan, and D. Chandler, Science **323**, 1309 (2009).
[5]M. D. Ediger, C. A. Angell, and S. R. Nagel, J. Phys. Chem. **100**, 13200 (1996).
[6]W. H. Wu, B. Ellman, T. F. Rosenbaum, G. Aeppli, and D. H. Reich, Phys. Rev. Lett. **67**, 2076 (1991).
[7]A. Amir, Y. Oreg, and Y. Imry, Phys. Rev. Lett. **103**, 126403 (2009).
[8]T. E. Markland, J. A. Morrone, B. J. Berne, K. Miyazaki, E. Rabani, and D. R. Reichman, Nat. Phys. **7**, 134 (2011).
[9]H. Westfahl, J. Schmalian, and P. G. Wolynes, Phys. Rev. B **68**, 134203 (2003).
[10]L. Cugliandolo and G. Lozano, Phys. Rev. Lett. **80**, 4979 (1998).
[11]L. Cugliandolo and G. Lozano, Phys. Rev. B **59**, 915 (1999).
[12]L. Cugliandolo, D. Grempel, and C. Santos, Phys. Rev. B **64**, 014403 (2001).
[13]G. Biroli and L. Cugliandolo, Phys. Rev. B **64**, 014206 (2001).

[14] L. Cugliandolo, D. Grempel, G. Lozano, H. Lozza, and C. Santos, Phys. Rev. B **66**, 014444.

[15] L. Cugliandolo, D. Grempel, G. Lozano, and H. Lozza, Phys. Rev. B **70**, 024422 (2004).

[16] L. F. Cugliandolo, Int. J. Mod. Phys. B **20**, 2795 (2006).

[17] L. Foini, G. Semerjian, and F. Zamponi, Phys. Rev. B **83**, 094513 (2011).

[18] W. Götze, *Complex Dynamics of Glass-Forming Liquids: A Mode-Coupling Theory* (Oxford University Press, Oxford, 2009).

[19] I. R. Craig and D. E. Manolopoulos, J. Chem. Phys. **121**, 3368 (2004).

[20] E. Rabani and D. R. Reichman, Annu. Rev. Phys. Chem. **56**, 157 (2005).

[21] R. Kubo, M. Toda, and N. Hashitsume, *Statistical Physics II, Solid State Sciences*, 2nd ed. (Springer, Berlin, 1995).

[22] W. Götze and M. Lücke, Phys. Rev. B **13**, 3822 (1976).

[23] J. S. Thakur and K. N. Pathak, in *International Centre for Theoretical Physics*, Publication IC/82/2 (Trieste, 1986).

[24] O. Kletenik-Edelman, D. R. Reichman, and E. Rabani, J. Chem. Phys. **134**, 044528 (2011).

[25] D. R. Reichman and E. Rabani, Phys. Rev. Lett. **87**, 265702 (2001).

[26] E. Rabani and D. R. Reichman, Phys. Rev. E **65**, 036111 (2002).

[27] D. R. Reichman and E. Rabani, J. Chem. Phys. **116**, 6279 (2002).

[28] E. Rabani and D. R. Reichman, J. Chem. Phys. **116**, 6271 (2002).

[29] E. Rabani, D. R. Reichman, G. Krilov, and B. J. Berne, Proc. Natl. Acad. Sci. U.S.A. **99**, 1129 (2002).

[30] E. Rabani and D. R. Reichman, Europhys. Lett. **60**, 656 (2002).

[31] E. Rabani and D. R. Reichman, J. Chem. Phys. **120**, 1458 (2004).

[32] E. Rabani, K. Miyazaki, and D. R. Reichman, J. Chem. Phys. **122**, 034502 (2005).

[33] E. Rabani, G. Krilov, D. R. Reichman, and B. J. Berne, J. Chem. Phys. **123**, 184506 (2005).

[34] W. Götze and M. Lücke, Phys. Rev. B **13**, 3825 (1976).

[35] H. W. Jackson and E. Feenberg, Rev. Mod. Phys. **34**, 686 (1962).

[36] R. P. Feynman and M. Cohen, Phys. Rev. **102**, 1189 (1956).

[37] W. Götze and L. Sjögren, Rep. Prog. Phys. **55**, 241 (1992).

[38] U. Balucani and M. Zoppi, *Dynamics of the Liquid State* (Oxford University Press, New York, 1994).

[39] E. Rabani and D. R. Reichman, J. Phys. Chem. B **105**, 6550 (2001).

[40] D. Chandler, Y. Singh, and D. M. Richardson, J. Chem. Phys. **81**, 1975 (1984).

[41] A. L. Nichols III, D. Chandler, Y. Singh, and D. M. Richardson, J. Chem. Phys. **81**, 5109 (1984).

[42] R. Collepardo-Guevara, I. R. Craig, and D. E. Manolopoulos, J. Chem. Phys. **128**, 144502 (2008).

[43] T. F. Miller and D. E. Manolopoulos, J. Chem. Phys. **122**, 184503 (2005).

[44] I. R. Craig and D. E. Manolopoulos, Chem. Phys. **322**, 236 (2006).

[45] T. E. Markland, S. Habershon, and D. E. Manolopoulos, J. Chem. Phys. **128**, 194506 (2008).

[46] Y. V. Suleimanov, R. Collepardo-Guevara, and D. E. Manolopoulos, J. Chem. Phys. **134**, 044131 (2011).

[47] J. O. Richardson and S. C. Althorpe, J. Chem. Phys. **131**, 214106 (2009).

[48] W. Kob and H. C. Andersen, Phys. Rev. E **51**, 4626 (1995).

[49] W. Kob and H. C. Andersen, Phys. Rev. E **52**, 4134 (1995).

[50] M. Ceriotti, M. Parrinello, T. E. Markland, and D. E. Manolopoulos, J. Chem. Phys. **133**, 124104 (2010).

[51] T. E. Markland and D. E. Manolopoulos, J. Chem. Phys. **129**, 024105 (2008).

[52] M. Parrinello and A. Rahman, J. Chem. Phys. **80**, 860 (1984).

[53] G. A. Voth, Adv. Chem. Phys. **93**, 135 (1996).

[54] M. Pavese and G. A. Voth, Chem. Phys. Lett. **249**, 231 (1996).

[55] T. D. Hone and G. A. Voth, J. Chem. Phys. **121**, 6412 (2004).

[56] K. Leung and D. Chandler, Phys. Rev. E **49**, 2851 (1994).

[57] *Hydrogen in Metals III: Properties and Applications*, edited by H. Wipf (Springer-Verlag, Berlin, 1997).